ENERGY DEPENDENCE OF ELECTRON TRAPPING IN A SOLAR FLARE

DAVID ALEXANDER and THOMAS R. METCALF
Lockheed Martin Solar and Astrophysics Laboratory, 3251 Hanover Street, Palo Alto, CA 94304, U.S.A.

(Received 8 August 2002; accepted 18 August 2002)

Abstract. Observations of an energy-dependent asymmetry in footpoint hard X-ray emission by RHESSI for the M4.0 solar flare of 17 March 2002 allows us to probe the dynamics of particle transport with energy and time. The presence of such an asymmetry is most readily explained by the effects of a converging magnetic field with different rates of convergence at the different footpoints, as would be expected from realistic surface field distributions. Such a geometry has been discussed in the context of a trap-plus-precipitation model where the transport of energetic particles in the flare is governed by the precipitation out of the coronal trap via collisions, wave-particle interactions or some other scattering process, into the high-density chromosphere. Comparison of RHESSI observations with a trap-plus-precipitation model allows us to use the energy dependence of the asymmetry and the observed ratio of footpoint to coronal emission at the different energies to assess the role of the trapping in the transport of energetic electrons and to probe the nature of the particle precipitation process inside the loss cone.

1. Introduction

Hard X-ray observations of solar flares provide important diagnostic information on the acceleration and subsequent transport of energetic particles in the solar corona. While it is now generally accepted that the bulk of the observed hard X-ray emission from flares is a result of the interaction of energetic electrons, accelerated in the corona, with the ambient medium via non-thermal electron bremsstrahlung, the details of the particle transport through the flaring solar atmosphere and the effects of the magnetic field geometry on this transport are still uncertain. Instrumentation on board a variety of spacecraft over the last two decades has generated a wealth of spectroscopic and imaging data which has significantly improved our understanding of the acceleration and transport processes in solar flares (see Aschwanden, 2002, for a recent and comprehensive review). The launch of RHESSI provides us with an unprecedented opportunity to explore the energy-dependence of the hard X-ray emission in space and time enabling new insight into the particle acceleration and transport processes.

In recent years much attention has been focused on the effects of coronal trapping, a natural consequence of the expected convergence of magnetic field between the corona, where the acceleration is presumed to occur, and the chromosphere where the bulk of the hard X-ray production is assumed to take place

Solar Physics **210:** 323–340, 2002.

(Brown, 1971). The idea of the magnetic trap in a solar context was originally proposed by Takakura and Kai (1966) and subsequently developed into the trap-plus-precipitation model by Melrose and Brown (1976) which was further refined by a series of authors (e.g., MacKinnon, 1988, 1991; Alexander, 1990; McClements, 1990a, b). One of the principal theoretical attractions of the trap model is that it circumvents the electrodynamic problems associated with the very large electron beam fluxes required to generate the observed blue shifts during the impulsive phases of solar flares (LaRosa and Emslie, 1988).

As observations have improved, considerable evidence in support of the trap-plus-precipitation scenario for energetic electrons in solar flares has accrued (Bai and Ramaty, 1979; Bai *et al.*, 1983; Bai and Dennis, 1985; Ramaty *et al.*, 1994; Alexander and Metcalf, 1997; Aschwanden *et al.*, 1999; Metcalf and Alexander, 1999). In particular, imaging observations at low energies (< 40 keV) have often shown hard X-ray emission located purely in the corona (Tsuneta *et al.*, 1984; Takakura *et al.*, 1987) with higher energy emissions concentrated at low altitudes (Kane, 1983; Aschwanden *et al.*, 1999). Less direct evidence for the need of a coronal trap lies in presence of a strong stationary component in soft X-ray emission lines (McClements and Alexander, 1989) contrary to what is expected from the thick-target electron beam interpretation of hard X-ray observations (e.g., Emslie and Alexander, 1987) which predicts large systematic blue shifts in these lines.

In this paper we are particularly interested in the exploration of the particle transport through the analysis of asymmetric trap geometries: a situation necessitated by the spatially resolved observations of asymmetric hard X-ray footpoints in a large number of solar flares. An asymmetric trap model was developed by Aschwanden *et al.* (1999) who used combined measurements from CGRO/BATSE (Fishman *et al.*, 1992) and the *Yohkoh*/HXT (Kosugi *et al.*, 1991) to quantify the relative fractions of the directly precipitating and trap-precipitating electrons at both magnetically conjugate footpoints. The presence of an asymmetry allows us to examine in detail the energy and time dependence of the particle transport.

When coupled to the increased sensitivity and improved energy resolution of RHESSI (Lin *et al.*, 2002), the characteristics of the observed asymmetry and its behavior with energy and time yield important clues to the physics governing the particle transport in solar flares. In this paper we address this issue via RHESSI observations of a solar flare which exhibited a well-defined and energy-dependent footpoint asymmetry and put these observations in context with the trap-plus-precipitation models. In Section 2 we present the observations and analysis while our results and interpretation are discussed in Section 3. Conclusions are subsequently presented in Section 4.

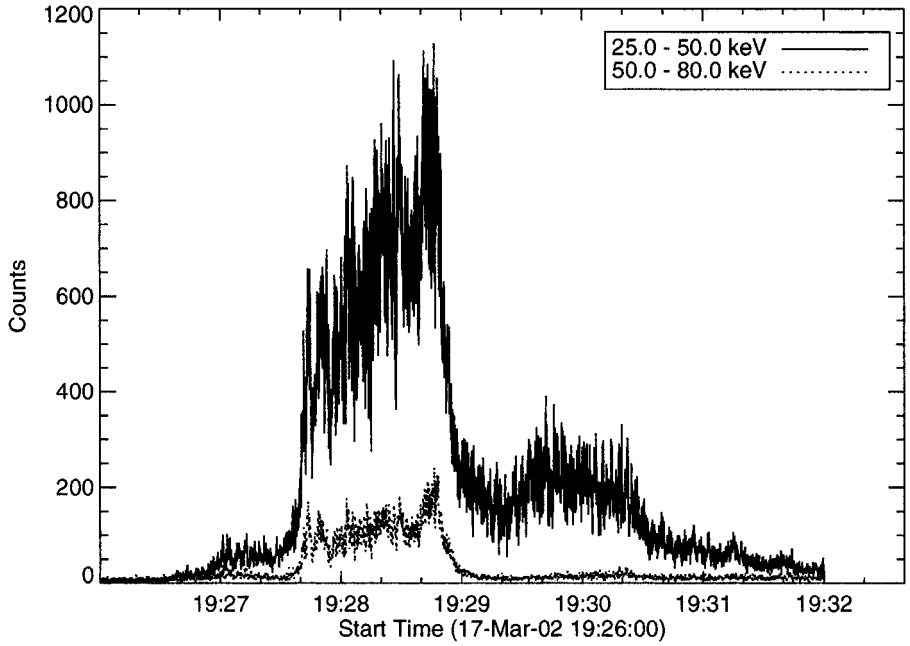

Figure 1. The light curve for the 17 March 2002 flare in two energy bands: 25–50 keV (*solid*) and 50–80 kev (*dotted*). The counts are summed into 0.1 s bins.

2. Observations and Analysis

RHESSI observed an M4.0 solar flare at 19:28 UT on 17 March 2002. The impulsive flare was in NOAA active region number 9871 at S21 E17. Figure 1 shows the hard X-ray light curve for this event. The analysis presented here is restricted to the flare impulsive phase from 19:27:30 through 19:29:00 UT. The inferred spectral index for this event is $\delta \approx 3.5$.

Figure 2 displays images in a subset of the energy bands considered. Images were reconstructed using the Pixon algorithm which gives the best suppression of spurious sources and hence the best photometry (Metcalf *et al.*, 1996). Energies above 30 keV are not shown since they are similar in appearance to the 28–30 keV image. The images shown in Figure 2 were reconstructed using the entire impulsive phase of the flare from 19:27:30 to 19:29:00 UT. To examine the time variability of the hard X-ray sources images were also reconstructed in time intervals from 19:27:30–19:28:00, 19:28:00–19:28:30, and 19:28:30–19:29:00 UT. All images were reconstructed using RHESSI detectors 3–9. The images show two distinct footpoint regions (east and west) and a coronal source (e.g., Masuda *et al.*, 1994) between the two footpoint regions and provide the basic data for the analysis described below.

For our investigation of the asymmetry in the hard X-ray emission from the two footpoint regions it is important to understand the character of the magnetic

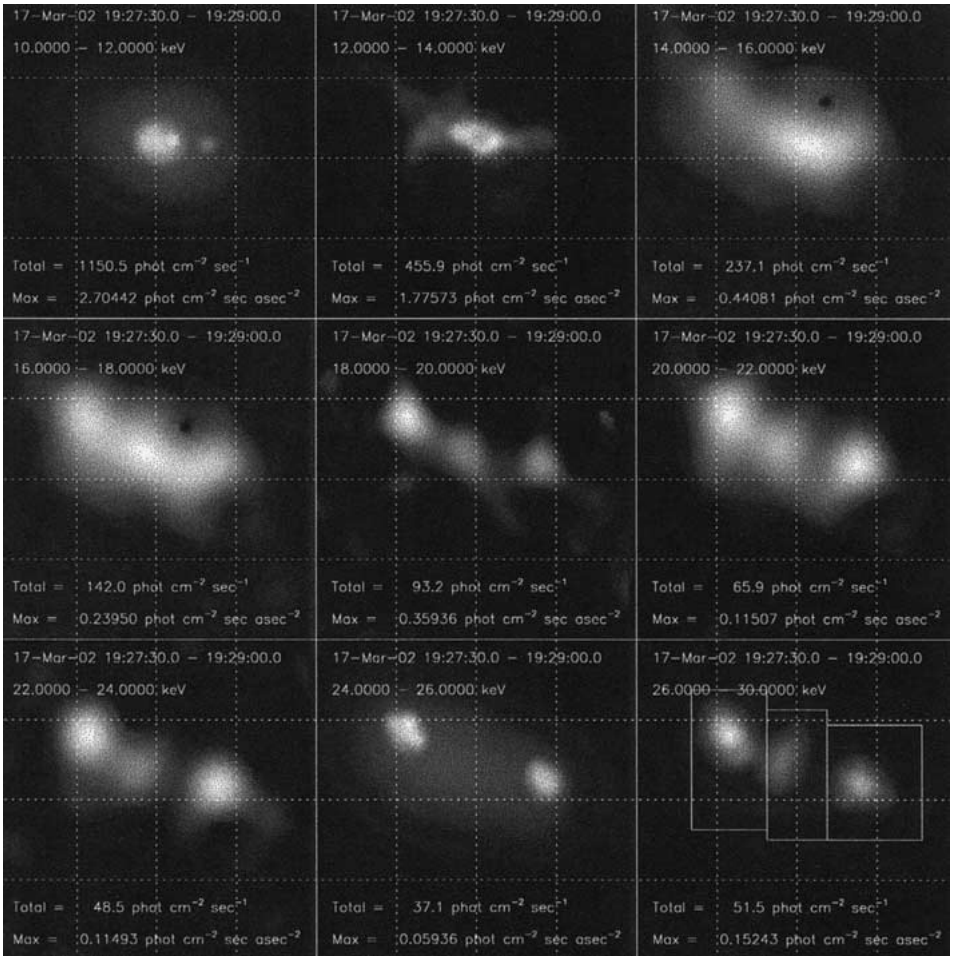

Figure 2. RHESSI images reconstructed using the Pixon algorithm in energy bands from 12 to 30 keV. At low energies the image is dominated by a coronal source. At high energies the images are dominated by two footpoint regions. In the *lower right* the boxes used to separate emission from the footpoints and the corona are shown. The images are each 64 arc sec × 64 arc sec with 1 arc sec pixels and are independently scaled. The total and maximum brightness for each image is given.

field at the footpoints. Figure 3 shows an overlay of the RHESSI hard X-rays on the SOHO/MDI (Scherrer *et al.*, 1995) photospheric vertical magnetic field. The vertical field was derived from the observed line-of-sight field using a simple potential field extrapolation. The MDI and RHESSI data were co-aligned using the known pointing of each instrument after correcting the MDI data for the parallax between the L1 view and the Earth view. The magnetic field in the vicinity of the west footpont is 650 G while the magnetic field in the vicinity of the east footpoint is quite variable since the footpoint sits at the edge of a strong spatial gradient in the magnetic field. The field in the vicinity of the east footpoint varies from −450 G

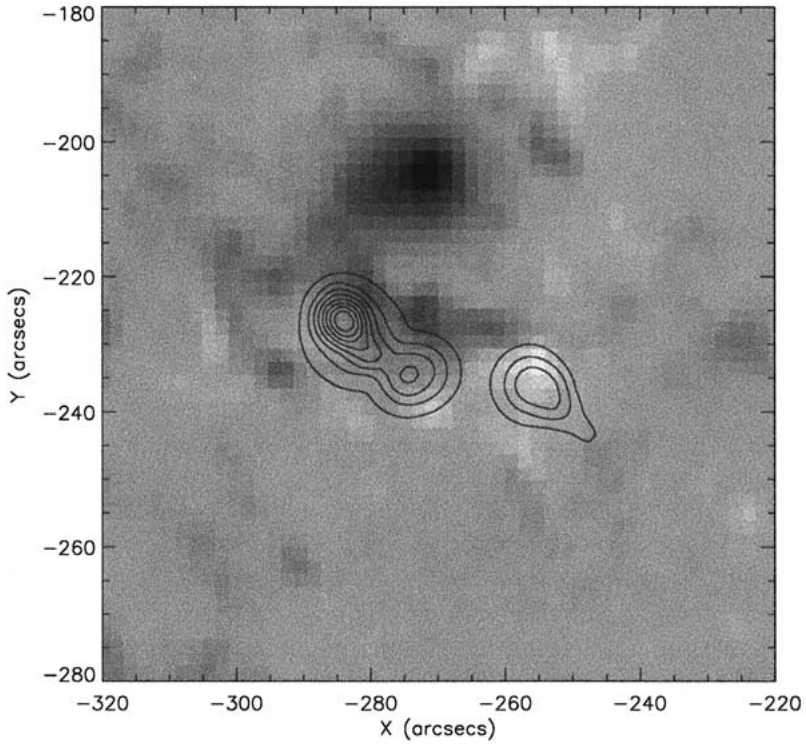

Figure 3. Contours of RHESSI hard X-ray emission (19:27:30–19:28:30 UT, 12–25 keV) overlayed on the MDI vertical magnetic field at 19:46:30 UT (*dark*: downward field, *white*: upward field).

to −1000 G depending on where the true flare footpoint is located. The spatial resolution achieved in the RHESSI images, and the uncertainty in the RHESSI pointing, make it difficult to determine the exact ratio of the magnetic field at the two footpoints. However, the range of possible values we derive is from 0.7 to 1.5 (west/east).

The asymmetry in the hard X-ray footpoint emission, A, is derived by summing the X-rays in boxes (Figure 2) surrounding the footpoints and computing the difference in brightness between the two footpoints divided by the sum of the brightness in the two footpoints, viz.,

$$A = \frac{I_2 - I_1}{I_2 + I_1}, \tag{1}$$

where I_i denotes the count rate at footpoint i. For perfect symmetry, $A = 0.0$ and for perfect asymmetry, $A = \pm 1.0$. Figure 4 shows the footpoint asymmetry for the early impulsive phase of the flare, 19:27:30–19:28:00 UT. Although there is a strong degree of scatter, there is evidence of a reduction in the asymmetry with increasing photon energy above 20 keV. A fit to the data above 20 keV, and excluding the last point at 70–80 keV where the count rates are small, yields an

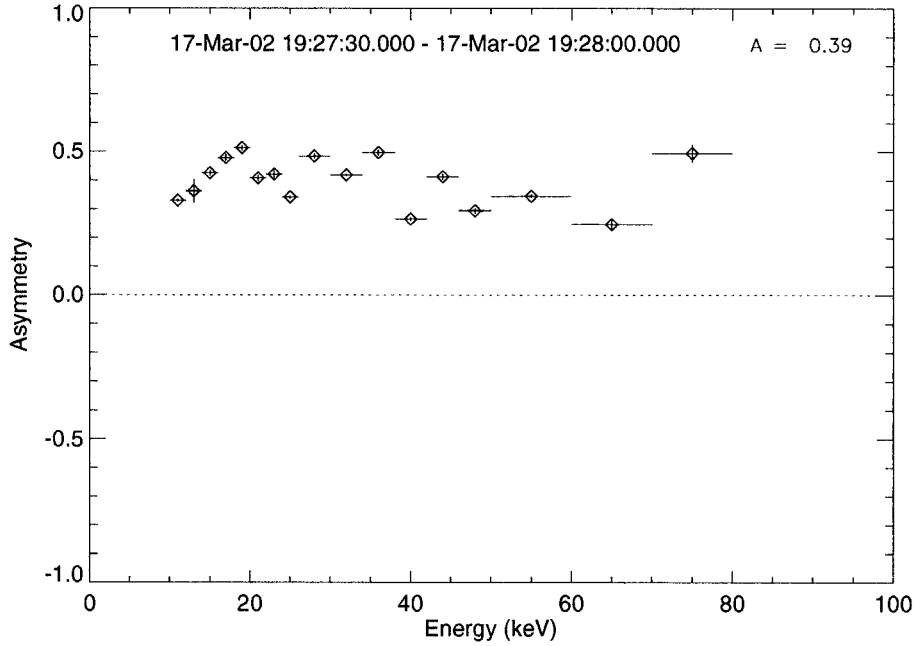

Figure 4. The asymmetry in the footpoint emission in the early impulsive phase from 19:27:30 to 19:28:00 UT, as a function of energy. The *horizontal bars* show the energy bands used and the *vertical bars* show the statistical errors. The energy integrated asymmetry is 0.39.

energy dependence of $4.1 \pm 1.4 \times 10^{-3}$ (keV)$^{-1}$, which is significant at the 3-sigma level. The quoted uncertainty was calculated from the scatter about the linear fit rather than from the statistical error bars which are considerably smaller than the scatter. The energy-integrated asymmetry is found to be $A_I = 0.39$. There is also some evidence for an increase in the asymmetry with energy at low photon energies ($\varepsilon < 20$ keV).

Late in the impulsive phase the character of the asymmetry clearly changes (Figure 5). From 19:28:00 to 19:28:30 UT, the asymmetry is reduced and from 19:28:30 to 19:29:00 UT the asymmetry has changed sign and shows a complex variation with energy. We will discuss this more fully in the following section.

Figure 6 shows the ratio, $R = I_{fp}/I_{\rm cor}$, of the footpoint emission to the emission from the corona, the latter being dominated by the Masuda-like source. Similar to the energy variation in the asymmetry, R shows a general decay with energy in the early impulsive phase as would be expected from the early development of the particle transport when R is dominated by directly precipitated electrons: higher energies stay in the trap longer. In the late impulsive phase, R is progressively reduced with time at low energies as the corona becomes bright via heating and chromospheric evaporation and as the once-trapped particle population grows to dominate the directly-precipitated particles in the loss cone. At higher energies, R is consistently of the order of 2.5, i.e., the combined hard X-ray emission from the

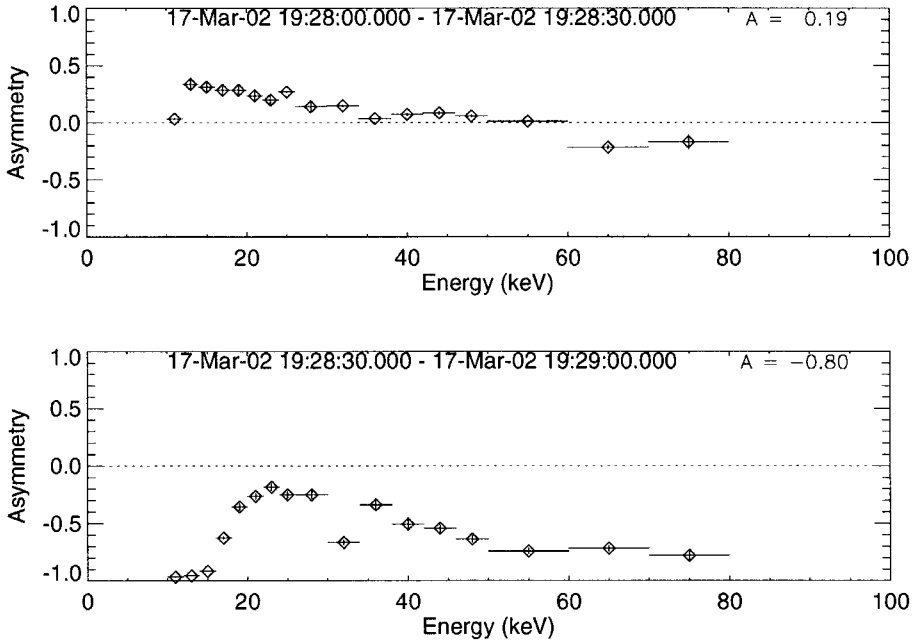

Figure 5. The asymmetry in the footpoint emission late in the impulsive phase from 19:28:00 to 19:28:30 UT (*upper plot*) and 19:28:30 to 19:29:00 UT (*lower plot*), as a function of energy. The *horizontal bars* show the energy bands used and the small *vertical bars* show the statistical errors.

two footpoint sources is about 2.5 times the emission from the corona. This demonstrates that, while the coronal emission is strongly influenced by the presence of a trap, the bulk of the emission at early times is dominated by directly precipitated particles.

The vertical bars in Figures 4–7 show the statistical errors on the asymmetry. These errors are derived from the uncertainties provided by the Pixon reconstruction algorithm and represent the statistical errors but do not represent any systematic errors which might be caused by the reconstruction itself.

Two things to bear in mind when interpreting the data shown in Figures 4–7 are the necessity of separating the coronal and footpoint emission and the requirement of potentially long ($\sim$ 30 s) image accumulation times (cf., Metcalf and Alexander, 1999). The selection of boxes invariably results in some coronal emission being defined as footpoint emission with the impacts that the observed asymmetry could be lower than the true value and that R is too high. This leads to lower inferred loss-cone angles and larger asymmetries implying a larger ratio of footpoint fields. Additionally, a 30 s accumulation time could be comparable to the trapping time for low energy electrons, depending upon the ambient density, resulting in a significant impact on the inferred asymmetry and emission ratio at these energies (see below). For stronger events we will be able to reduce the image accumulation times significantly.

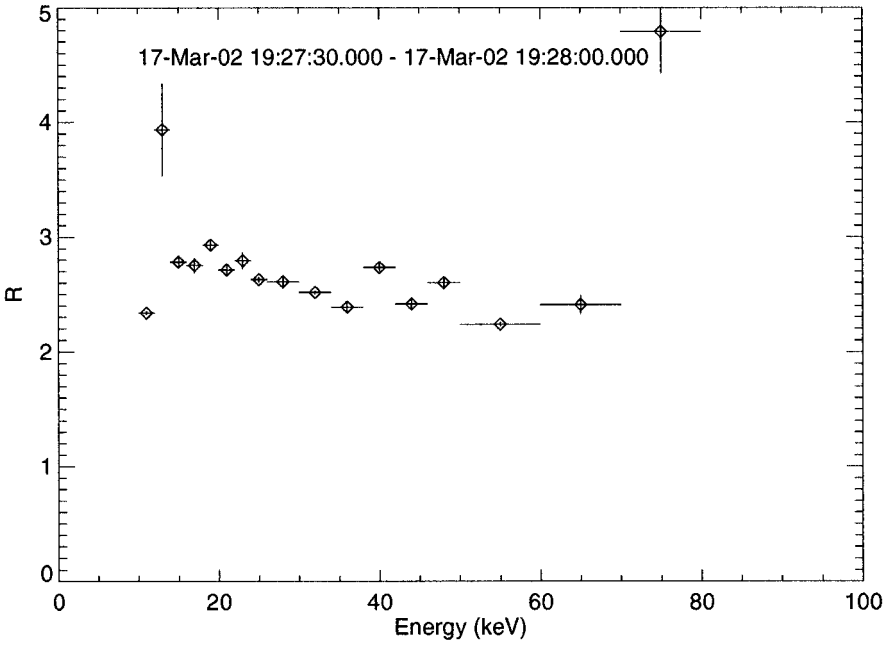

Figure 6. The ratio of the footpoint emission to the coronal emission as a function of energy early in the impulsive phase. The *horizontal bars* show the energy bands used and the small *vertical bars* show the statistical errors.

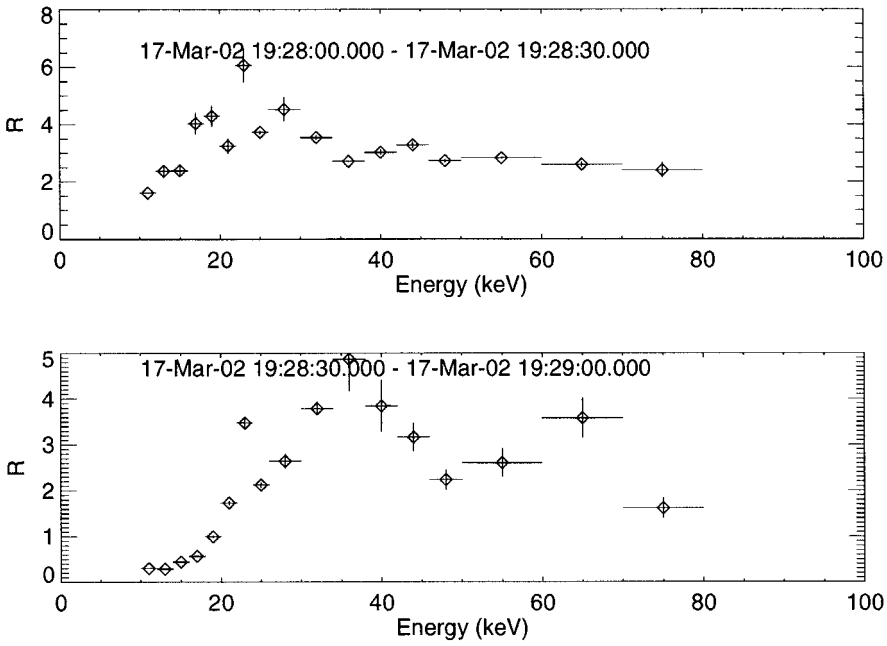

Figure 7. The ratio of the footpoint emission to the coronal emission as a function of energy late in the impulsive phase. The *horizontal bars* show the energy bands used and the small *vertical bars* show the statistical errors.

3. Results and Discussion

The analysis discussed in the preceding section demonstrates a clear asymmetry in the hard X-ray emission emanating from the footpoints of the flaring loop. Below we will discuss the energy and time dependence of this asymmetry, and the subsequent spatial distribution of the hard X-ray emission, but it should be noted that the mere presence of an asymmetry alone provides us with a powerful diagnostic tool for understanding the particle transport in this flare (cf., Aschwanden *et al.*, 1999).

As we will show, comparison of the observed asymmetry and hard X-ray spatial distribution with existing trap-plus-precipitation models (e.g., McClements, 1990a, b; MacKinnon, 1991) for non-thermal electrons allows us to use the observed asymmetry to constrain the loss-cone angles responsible for the hard X-ray emission in the conjugate footpoints. Moreover, the observed ratio of coronal ('trapped') to footpoint ('precipitated') hard X-ray emission provides an additional derivation of the loss-cone angles which can be readily compared with those derived from the asymmetry.

3.1. Modeling the asymmetry

In this paper we assume that the unspecified acceleration process generates an energetic particle population which is isotropic in pitch angle space (cf., Alexander, 1990; McClements, 1990a) and is symmetrically injected into either side of the loop. Any accelerated particle distribution with a highly anisotropic injection profile, at either large, e.g., MacKinnon (1988), or small, e.g., electron beam model of Brown (1971), pitch angles would likely be rapidly isotropized by plasma instabilities (e.g., Holman, 1985). McClements (1990a) demonstrated clearly that the spatial distribution of the hard X-ray emission predicted by the trap-plus-precipitation model is strongly dependent on the pitch-angle distribution of the accelerated electrons and so it is important to represent the accelerated population as realistically as possible.

Figure 4 shows that early in the impulsive phase there is a strong asymmetry in the emission from the conjugate footpoints of the flaring loop. There is clear evidence for an energy dependence in this asymmetry (not found by Aschwanden *et al.*, 1999, using *Yohkoh*/HXT data). However, in this section, we will concentrate on the energy-integrated asymmetry which was found to be $A_I = 0.39$.

We define the asymmetry as in Equation (1) with I_1 and I_2 being defined here as the directly precipitated fluxes at each of the two footpoints; we are implicitly assuming that early in the impulsive phase the footpoint hard X-ray production is dominated by directly precipitating electrons. This is a slightly different definition of the asymmetry than used by Aschwanden *et al.* (1999): $A_{\mathrm{Asch}} = I_2/(I_1 + I_2)$. The asymmetry defined in Equation (1) is simply $A = 2A_{\mathrm{Asch}} - 1$.

The magnetic field is assumed to have a uniform value B_{cor} in the corona, increasing rapidly to a value $B_{\mathrm{chrom},1}$, $B_{\mathrm{chrom},2}$ at each of the loop footpoints re-

spectively (cf., MacKinnon, 1988). With this definition the loss-cone angle takes the form

$$\theta_{0i} = \sin^{-1}\left(\frac{B_{\rm cor}}{B_{{\rm chrom},i}}\right)^{1/2}, \tag{2}$$

where $i \in (1, 2)$ denotes the particular footpoint of interest, and is uniquely defined throughout the coronal part of the loop. Assuming isotropic injection with a source function given by

$$S(E, \sigma) = s_0 E^{-\delta} \frac{\sigma}{(1-\sigma^2)^{1/2}} \equiv s_0 E^{-\delta} f(\sigma), \tag{3}$$

where $\sigma = \sin\theta$ is the pitch-angle sine (see Alexander, 1990), we can obtain the asymmetry by only considering electrons with pitch angles $\theta < \theta_{02}$. The source function S defined in Equation (3) denotes the injection rate per unit σ. This results in an injection rate per unit solid angle which is independent of the pitch angle, θ. Particles injected towards footpoint 1 with pitch angles $\theta_{01} < \theta < \theta_{02}$ will precipitate at footpoint 2 after a single bounce at mirror point 1. This is the source of the observed asymmetry at early times.

Ignoring the details of the photon production, the photon emission at each footpoint is given by

$$I_1 = \text{ const. } \times \int_0^{\sigma_{01}} f(\sigma)\, {\rm d}\sigma = \int_0^{\theta_{01}} \sin\theta\, {\rm d}\theta = 1 - \mu_{01}, \tag{4}$$

$$I_2 = \text{ const. } \times \int_0^{\sigma_{02}} f(\sigma)\, {\rm d}\sigma + \int_{\sigma_{01}}^{\sigma_{02}} f(\sigma)\, {\rm d}\sigma = 1 + \mu_{01} - 2\mu_{02}, \tag{5}$$

yielding an asymmetry

$$A = \frac{I_2 - I_1}{I_2 + I_1} = \frac{\mu_{01} - \mu_{02}}{1 - \mu_{02}}, \tag{6}$$

where $\sigma_{0i} = \sin\theta_{0i}$, and $\mu_{0i} = \cos\theta_{0i}$. We have further assumed that the distribution of those particles with pitch angles $\theta_{01} < \theta < \theta_{02}$ does not undergo significant modification during their single 'bounce' from the mirror point at $B_{{\rm chrom},1}$ to the loss cone defined by θ_{02}.

Our definition of the theoretical asymmetry, A, assumes no effects due to Coulomb collisions in the loss cone. This is a good assumption, except at very small energies, since the loss cone is effectively empty for energies greater than ~ 6 keV in the corona; the energy at which the loop transit time equals the collisional pitch angle scattering time. Therefore, assuming identical injection profiles into both sides of the flaring loop, our asymmetry is defined to first order by the form above (see MacKinnon, 1991). Moreover, our theoretical asymmetry is really only valid

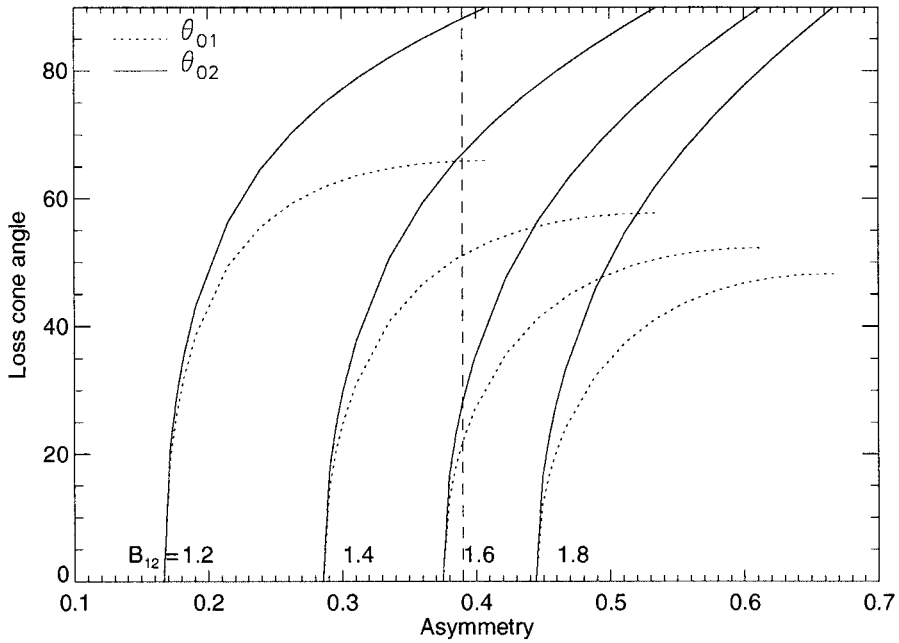

Figure 8. The relationship between the loop loss-cone angles and the asymmetry for different values of the footpoint magnetic field ratio. The *dashed line* indicates the observed value of the energy-integrated asymmetry, $A_I = 0.39$.

for short times such that the footpoint emission is dominated by the flux of directly precipitated electrons, before significant scattering from the trap has occurred, and assuming no pitch-angle dependence with time of the injected particle distribution.

From Equation (2) we obtain the relationship between the asymmetric loss-cone angles and the ratio of the magnetic field at the conjugate footpoints:

$$\left(\frac{\sigma_{02}}{\sigma_{01}}\right)^2 = \frac{B_{\mathrm{chrom},1}}{B_{\mathrm{chrom},2}} \equiv B_{12}. \tag{7}$$

Figure 8 illustrates the relationship between the loss-cone angles and the asymmetry for a given footpoint field ratio, B_{12}. The measured range of $0.7 < B_{12} < 1.5$ limits the asymmetry to $A < 0.56$ with $I_2 > I_1$ and for asymmetries as high as 0.53 if the footpoint asymmetry switches such that $I_1 > I_2$. The observed energy-integrated asymmetries at the beginning of the impulsive phase ($A_I = 0.39$) would suggest that $1.2 \leq B_{12} \leq 1.6$, since higher values do not accommodate asymmetries as low as 0.39 in this pre-scattering limit. A more certain measurement of the magnetic field at the footpoints would have enabled us to determine the loss-cone angles directly from the measured asymmetry, thereby yielding the field convergence on each side of the loop and providing an estimate of the magnetic field in the corona.

In the absence of a well-defined footpoint field, particularly at the eastern footpoint (see Section 2), we can use the measurement of the spatial distribution of the hard X-ray emission to provide an independent inference of the loss-cone angles. Comparison with the dispersive calculation of McClements (1990a), shows that the energy integrated value of $R_I = 2.5$ would correspond to a loss-cone angle of $\theta_0 \sim 53^\circ$ (McClements, 1990a, defines $R = I_{cor}/I_{fp}$ as the ratio of the coronal to the footpoint emission). Taking θ_0 as an average loss-cone angle, the observed asymmetry indicates that $B_{12} \simeq 1.44$ with $\theta_{01} = 46^\circ$ and $\theta_{02} = 61^\circ$, assuming that we are only observing effects from directly precipitating electrons in the early phase of the flare. Using these values for the loss cone and our determination of B_{12} we can estimate that for this flaring structure the magnetic field in the corona is of order 170 G, where we assume that the chromospheric field where the particles thermalize is 50% of the measured photospheric field. This value is high but reflects the large loss-cone angles inferred from the large asymmetries in the RHESSI footpoint fluxes.

The high values of R seen in Figure 6 imply a weak convergence of the magnetic field in the coronal loop (McClements, 1990a). It is interesting to note that Melrose and Brown (1976) obtained the result

$$\frac{4}{\delta + 2} < R < 2, \tag{8}$$

where δ is the electron energy spectral index. The high observed values, $R > 2$, indicate that the energy loss and pitch-angle scattering due to Coulomb collisions, neglected by Melrose and Brown (1976), are important for the particle transport in the trapped portion of the loop.

The asymmetric trap analysis of Aschwanden *et al.* (1999) obtains statistical averages for the loss cone angles from a data set of some 54 flares. Similar to the values quoted in the present work, they find $\theta_{01} = 42^\circ \pm 11^\circ$ and $\theta_{02} = 52^\circ \pm 10^\circ$, where subscript '1' denotes the less bright footpoint, yielding mirror ratios $1.6 < B_{\mathrm{chrom},1}/B_{\mathrm{cor}} < 4.0$ and $1.3 < B_{\mathrm{chrom},2}/B_{\mathrm{cor}} < 2.5$, respectively. The ratio of footpoint field by Aschwanden *et al.* (1999), $B_1/B_2 \sim 1.2$ with a range of 1.1–1.8, inferred from the measured asymmetry, is consistent with measured ratio here (see Figure 3).

3.2. Energy dependence of asymmetry and flux ratio

Although the loss-cone angle is completely specified by the field convergence as per Equation (2) and the mirror point is strictly a function of the particle's pitch angle and not its energy, the presence of collisional pitch angle scattering and energy loss introduce an energy dependence in the precipitation rate, particularly at later times. The isotropic injection solution for the ratio of footpoint to coronal emission, derived from the fully-dispersive calculation of McClements (1990a), exhibited a weak dependence of R on energy, with R varying by $\leq 20\%$ between

photon energies, $\varepsilon = 20$ keV and $\varepsilon = 200$ keV. From Figure 6 we find a stronger dependence with R varying by $\sim 25\%$ between 20 keV and 60 keV. Aschwanden *et al.* (1999) found little variation in the asymmetry, averaged over 29 flares with well-separated footpoints, at different energies using BATSE and *Yohkoh*/HXT: $A_{23-33}/A_{14-23} = 0.96 \pm 0.07$ and $A_{33-53}/A_{23-33} = 1.06 \pm 0.18$.

Figure 4 shows that during the impulsive phase there is an energy dependence in the asymmetry with A decreasing as we move to higher energies: from 0.5 at $\varepsilon = 20$ keV to 0.35 at $\varepsilon = 60$ keV. This trend of larger asymmetry at lower energies would be expected from the energy dependence of the Coulomb collisional scattering, with preferential scattering into the larger loss cone.

The footpoint-to-coronal-flux ratio shows a weak energy dependence, with R decreasing from $R \sim 2.9$ to $R \sim 2.3$ as ε increases from 20 keV to 60 keV. A simple application of the energy integrated results of McClements (1990a), assuming the loss cone angles derived from the energy dependence of the asymmetry, would suggest a variation of R much greater than that observed ($R_{69^\circ} > 5$; $R_{42^\circ} \sim 1$). Clearly, a more targeted investigation combining the RHESSI observations with theoretical calculations is required before we can utilize the observed energy dependence of the spatial distribution of the hard X-ray emission to fully understand the particle transport in solar flares. The results presented here provide a strong basis from which to build such an investigation.

At low electron energies for which the loop transit time is comparable to the collisional energy loss time, $E \sim 6$ keV, the weak diffusion limit does not apply and we must consider the energy losses and pitch-angle scattering which occur as the electrons traverse the corona within the loss cone. The consequence is that we might expect to see a fall off of R with decreasing energy. There is some slight evidence for this during the start of the impulsive phase (Figure 6) which gets stronger as time proceeds (Figure 7) and as the trapped particles start to enter the loss cone. In the dispersive calculation of McClements (1990a) there are a significant number of low energy electrons for which the loss-cone escape time is sufficiently long to be comparable to the electron collisional loss time and, consequently, these electrons may be ejected from the loss cone, thereby reducing the precipitation rate at these energies. Since the larger loss-cone will suffer from proportionately more degradation as low energy electrons are scattered out of the loss-cone, the effect of this will be to lower the asymmetry and the footpoint to corona emission ratio as is evident in Figures 4 and 6, particularly at later times (Figures 5 and 7).

A complication at late times is the dynamic development of the coronal plasma as the energy deposition heats and evaporates the chromosphere. The evolution of the source region as the heating develops and the density in the loop increases, skews the determination of R, especially at low energies. Thus, if we are truly to determine R from observations we should observe as early in the impulsive phase as count rates allow. As a result, the complex behavior in Figure 7 is less amenable to the analysis presented here.

On timescales shorter than the trapping times for electrons with $E > 20$ keV (cf., Metcalf and Alexander, 1999) no dependence on the energy spectrum is expected in the ratio of footpoint to coronal emission when the loss cone is subject to the weak diffusion limit (Kennel and Petschek, 1966; MacKinnon, 1988), defined by the loop transit time, t_e, being much shorter than the pitch-angle scattering time, t_s. However, in the strong limit, $t_s \leq t_e$, $R \sim \epsilon^2$, which is not observed except perhaps at low energies near the peak of the impulsive phase (19:28:00–19:29:00 UT, see Figure 7).

Finally, we note that in this paper we have ignored the spectral properties of the injected electron distribution (cf., Metcalf and Alexander, 1999) but calculations of the spatial distribution of hard X-ray emission in most of the extant models have been shown to only exhibit a very weak dependence on the spectral index.

3.3. Time dependence of asymmetry and flux ratio

In order to get good photometry when reconstructing hard X-ray images from the RHESSI data one has to integrate over times, typically of order 10–30 s depending upon the strength of the flare. For the event discussed here our image accumulation time is 30 s. This has a direct impact on the interpretation of the observed energy dependence in the asymmetry and flux ratio parameters (Alexander and Metcalf, 1997; Metcalf and Alexander, 1999). The time spent in a coronal trap where the dominant scattering mechanism is Coulomb collisions is energy dependent with the form

$$t_{\rm trap} = 0.95 \times 10^8 \left(\frac{E^{3/2}}{n_e}\right)\left(\frac{20}{\ln \Lambda}\right) \text{ s}, \tag{9}$$

where E is the electron energy in keV, n_e is the ambient electron density (cm^{-3}), and $\ln \Lambda$ is the Coulomb logarithm. Thus, a 100 keV electron will remain in the trap for ~ 11 times longer than a 20 keV electron and the trapping time for a 20 keV electron is $\sim 85(10^8/n_e)$ s. Assuming the ambient density early in the flare is low $\sim 2 \times 10^8$ cm^{-3}, then low energy electrons should leave the trap in about 45 s. We, therefore, assume that the results depicted in Figure 4 are uninfluenced by the trapping and the arguments in the preceding sections apply. However, precipitation of particles from the trap will have a marked effect on the inferred asymmetries and flux ratios at later times (Figures 5 and 7).

Metcalf and Alexander (1999) discussed a range of possible consequences related to the comparison of the various timescales in the trap-plus-precipitation problem. They found that if the image accumulation time, required to recover a high-confidence image reconstruction, was large relative to the trapping time then the average spectrum in the trap is harder than the injected spectrum by a power of ~ 1.5. Conversely, if the accumulation time was short compared to the trapping time the inferred spectrum in the trap would be identical to the injected spectrum but would harden with time as lower energy electrons escape the trap before the higher-energy electrons.

Precipitation from the trap over the relatively long integration times mean that we would measure an R 'contaminated' by pre-trapped particles. Since collisional deflection is an accumulation of small-angle scattering with the escape probability higher on the side of the loop with the larger loss-cone angle/weaker field (Aschwanden *et al.*, 1999), electrons scattered from the trap will tend to increase the asymmetry, A, and the footpoint/corona emission ratio, R, particularly at low energies. Consequently, the loss-cone angles inferred from these quantities are higher than would be derived from a distribution uninfluenced by significant pre-trapped electrons (Figure 8).

Figures 5 and 7 show the behavior of the asymmetry and flux ratio with energy as we progress to later times during the flare impulsive phase. Over the time range from 19:28:00 UT to 19:29:00 UT the asymmetry shows a transition from the clear dominance of one footpoint to the clear dominance of the other. The most likely explanation for this is that, as the flare develops, more loops begin to participate in the flaring. This is confirmed by the study of this event by Krucker and Lin (2002) in this volume, where there is a clear transition to different footpoints with an opposite sense of asymmetry. As was pointed out in Section 2 the eastern footpoint lies in a region of strong magnetic gradient (Figure 3) and, given that both footpoints lie in comparably strong magnetic fields, it is not unreasonable to suppose that a newly flaring loop in the same region might have dramatically different footpoint field ratios. The effect on the observed energy dependence of the asymmetry is quite marked as can be seen in Figure 5 and would require a much more sophisticated modeling than is currently available. Consequently we will forego discussion of the asymmetry at late times here and concentrate on the footpoint to coronal flux ratio.

As can be seen in Figure 7, the ratio of footpoint to coronal emission demonstrates some interesting behavior as we progress through the impulsive phase. Although we believe that there is a transition to different loop structures with different conjugate field properties, this should not have as strong an effect on the footpoint to coronal emission as it did for the asymmetry. This statement is based on the assumption that, whatever the field connectivity, the acceleration process and, consequently, the properties of the injected energetic particle distribution remain unchanged throughout this transition. Essentially, this constitutes a series of traps with the same particle injection profile, which significantly affects the observed asymmetries but not the flux ratios. We, thus, assume that the observed behavior of R with time is a direct consequence of the escape of particles from the trap into the loss cone.

The first thing to notice is that, compared to the early impulsive phase, R increases significantly at all but the lowest and highest energies, signifying an increase in the footpoint emission relative to that in the corona. The decrease observed at the lowest energies is a direct consequence of the increased density in the trap as chromospheric evaporation proceeds and the temperature increases (MacKinnon, 1986; Antonucci *et al.*, 1998). This results in more of the electrons

thermalizing in the corona, regardless of their pitch angles. As one would expect, the effect of this process with time would be to continue lowering R and having the degradation of R spread to higher energies, as is seen in a comparison between the top and bottom panels of Figure 7. Ultimately, the coronal emission comes to dominate the footpoint emission at low energies, $R < 1$, as is frequently observed (Antonucci *et al.*, 1998).

The enhancement in the flux ratio at energies 20–30 keV (19:28:00–19:28:30 UT) and 30–45 keV (19:28:30–19:29:00 UT), prior to the increasing density affecting these energies, can be understood in terms of the escape of particles from the trap into the loss cone, enhancing the footpoint emission at the expense of the coronal emission. Electrons with energies in the 20–30 keV range have trapping times of order 45–83 s for our assumed density of 2×10^8 cm^{-3}, comparable to the 60 s time from the beginning of the impulsive phase considered in the top panel of Figure 7 (slightly higher density at this time would lower these escape times). Electrons in the 30–45 keV energy range would have trapping times as long as $\sim 150(2 \times 10^8/n_e(t = 19{:}29))$ s, which compares with the 90 s time into the event considered in the bottom panel of Figure 7.

At the highest energies, $\varepsilon \gtrsim 65$ keV there is little change in R with time indicating that the trapped particles at these energies have not yet escaped the trap, having trapping times in excess of 260 s. Overall, the variation of R with time and energy would seem to match qualitatively the expected evolution of energetic particles in a trap-plus-precipitation scenario.

MacKinnon (1991) calculates the ratio of footpoint to trapped emission as a function of energy and time with the assumption that the source function for the injected accelerated particles is time dependent, effectively shutting off after a time $t = 2t_0$. He finds that at long times $t > 2t_0$ the ratio of footpoint to coronal hard X-ray emission decreases with increasing energy. Physically, this behavior is a result of the change in dominance of directly-precipitated particles to trap-precipitated particles as the injection rate falls to zero. While we have no direct indication of the time dependence of the injected profile from our data, the presence of a strong asymmetry over the whole of the impulsive phase suggests that the injection continues for $t_0 \gtrsim 30$ s. Over the energy range covered in our RHESSI analysis (12–60 keV) we expect R to fall from a value ~ 4 to ~ 2–3, extrapolating the curves of MacKinnon (1991). This is close to the observed behavior shown in Figures 6 and 7, indicating that trapping played a strong role in the hard X-ray source evolution for this event at late times.

4. Conclusions

The trap-plus-precipitation model has been with us for some time now. The new RHESSI solar flare observations enable us to study observationally the predictions and implications of this model with unprecedented energy and spatial resolution.

Our observations of the energy-dependent coronal emission and the asymmetry in the footpoint hard X-ray emission for the 17 March 2002 flare provide a new look at how electrons are trapped in the solar corona during flares and show that trapping played a significant role in the hard X-ray source evolution for this event. Observations of the coronal trap may be intimately connected with the particle acceleration process. For example, Tsuneta and Naito (1998) demonstrate how electrons can be accelerated through a first-order Fermi process at the fast shock: the region between fast- and slow-mode shocks trap the electrons.

The observations presented above are consistent with the trap-plus-precipitation model in which a portion of the coronal electron population is trapped as a result of the converging magnetic field in the transition region and chromosphere. The asymmetry in the footpoint emission early in the impulsive phase, combined with the ratio of the footpoint to coronal emission, predicts loss cone angles at the two footpoints of about 46 and 61 deg for the western and eastern footpoints, respectively. The small 15-deg difference in the loss cone angles well describes the observations early in the impulsive phase.

Later in the impulsive phase, the asymmetry changes sign. This is likely to be the result of the flare lighting up new magnetic field lines as time progresses so that the new field lines sample an ever shifting magnetic environment at the footpoints. For the observed flare, we surmise that the magnetic field strength at the west footpoint increases as the footpoint moves until the field at the western footpoint becomes larger than the field at the eastern footpoint. This is fully consistent with the MDI magnetic field observations which show a strong spatial gradient in the magnetic field at the western footpoint.

This study has pointed out some aspects of the data analysis to expand upon as we continue using RHESSI data to study the transport of flare particles. First, a more intense hard X-ray flare than the M4.0 described here will enable us to extend this work to shorter time integrations without sacrificing energy resolution. With these shorter time integrations, we will be able to study the dynamics of the trapped particles more directly if the time resolution can be set below the trapping time for the trapped particles. Further, we have not yet fully exploited the spectral characteristics of this event, a study which will also yield new insight into the trapped particle population.

Acknowledgements

We would like to thank the RHESSI team for their excellent work in providing a great scientific instrument and the software tools to access and analyze the data and to Säm Krucker for useful discussions. We are also particularly grateful to the referee for a rapid and insightful review. This work was supported in part by NASA grant NAS5-02048 (DA) and a direct grant from UC Berkeley (TRM).

References

Alexander, D.: 1990, *Astron. Astrophys.* **235**, 431.
Alexander, D. and Metcalf, T. R.: 1997, *Astrophys. J.* **489**, 442.
Antonucci, E. *et al.*: 1998, in J. L. R. Saba, B. M. Haisch, and J. T. Schmelz (eds.), 'Flare Dynamics', *The Many Faces of the Sun*, pp. 331–393.
Aschwanden, M. J.: 2002, *Space Sci. Reviews* **101**, 1.
Aschwanden, M. J., Fletcher, L., Sakao, T., Kosugi, T., and Hudson, H.: 1999, *Astrophys. J.* **517**, 977.
Aschwanden, M. J., Hudson, H. S., Kosugi, T., and Schwartz, R. A.: 1996, *Astrophys. J.* **464**, 985.
Bai, T. and Dennis, B. R.: 1985, *Astrophys. J.* **292**, 699.
Bai, T. and Ramaty, R.: 1979, *Astrophys. J.* **227**, 1072.
Bai, T., Hudson, H. S., Pelling, R. M., Lin, R. P., Schwartz, R. A., and von Rosenvinge, T. T.: 1983, *Astrophys. J.* **267**, 433.
Brown, J. C.: 1971, *Solar Phys.* **18**, 489.
Emslie, A. G. and Alexander, D.: 1987, *Solar Phys.* **110**, 295.
Holman, G. D.: 1985, *Astrophys. J.* **293**, 584.
Fishman, G. J., Meegan, C. A., Wilson, R. B., Paciesas, W. S., and Pendleton, G. N.: 1992,'The BATSE Experiment on the Compton Gamma Ray Observatory: Status and some Early Results', *The Compton Observatory Science Workshop*, pp. 26–34.
Kane, S.: 1983, *Solar Phys.* **86**, 355.
Kennel, C. F. and Petschek, H. E.: 1966, *J. Geophys. Res.* **71**, 1.
Kosugi T. *et al.*: 1991, *Solar Phys.* **136**, 17.
Krucker, S. and Lin, R. P.: 2002, *Solar Phys.* (this volume).
LaRosa, T. N. and Emslie, A. G.: 1988, *Astrophys. J* **326**, 997.
Lin R. P. *et al.*: 2002, *Solar Phys.*, this volume.
MacKinnon, A. L.: 1986, *Astron. Astrophys.* **163**, 2391.
MacKinnon, A. L.: 1988, *Astron. Astrophys.* **194**, 279.
MacKinnon, A. L.: 1991, *Astron. Astrophys.* **242**, 256.
Masuda, S., Kosugi, T., Hara, H., Tsuneta, S., and Ogawara, Y.: 1994, *Nature* **371**, 495.
McClements, K. G.: 1990a, *Astron. Astrophys.* **230**, 213.
McClements, K. G.: 1990b, *Astron. Astrophys.* **234**, 487.
McClements, K. G.: 1992, *Astron. Astrophys.* **253**, 261.
McClements, K. G. and Alexander, D.: 1989, *Solar Phys.* **123**, 161.
Melrose, D. B. and Brown, J. C.: 1976, *Monthly Notices Royal Astron. Soc.* **176**, 15.
Metcalf, T. R. and Alexander, D..: 1999, *Astrophys. J.* **522**, 1108.
Metcalf, T. R., Hudson, H. S., Kosugi, T., Puetter, R. C., and Piña, R. K.: 1996, *Astrophys. J.* **466**, 585.
Ramaty, R., Schwartz, R. A., Enome, S., and Nakajima, H.: 1985, *Astrophys. J.* **436**, 941.
Scherrer, P. *et al.*: 1995, *Solar Phys.* **162**, 129.
Takakura, T. and Kai, K.: 1966, *Publ. Astron. Soc. Japan* **18**, 57.
Takakura, T., Tanaka, K., Nitta, N., Kai, K., and Ohki, K.: 1987, *Solar Phys.* **107**, 109.
Tsuneta, S. and Naito, T.: 1998, *Astrophys. J.* **495**, L67.
Tsuneta, S. *et al.*: 1984, *Astrophys. J.* **280**, 887.